AGU100 ADVANCING EARTH AND SPACE SCIENCE

Geophysical Research Letters

RESEARCH LETTER
10.1029/2018GL079085

Key Points:
- Model experiments show that the nonlinearity of ENSO can weaken the ENSO amplitude under global warming
- Increased upper ocean thermal stratification inhibits thermocline depth variations and nonlinear temperature responses
- Observations exhibit stronger thermal stratification than models, suggesting that nonlinear ENSO weakening may occur in the real world

Supporting Information:
- Supporting Information S1

Correspondence to:
T. Kohyama,
kohyama@uw.edu

Citation:
Kohyama, T., Hartmann, D. L., & Battisti, D. S. (2018). Weakening of nonlinear ENSO under global warming. *Geophysical Research Letters*, *45*. https://doi.org/10.1029/2018GL079085

Received 6 NOV 2017
Accepted 27 JUL 2018
Accepted article online 6 AUG 2018

©2018. American Geophysical Union. All Rights Reserved.

Weakening of Nonlinear ENSO Under Global Warming

Tsubasa Kohyama[1], Dennis L. Hartmann[2], and David S. Battisti[2]

[1]Department of Earth and Planetary Science, The University of Tokyo, Tokyo, Japan, [2]Department of Atmospheric Sciences, University of Washington, Seattle, WA, USA

Abstract The amplitude response of the El Niño–Southern Oscillation (ENSO) to global warming is examined in two global climate models with realistic ENSO nonlinearity. Geophysical Fluid Dynamics Laboratory Earth System Model Version 2M (GFDL-ESM2M) and Model for Interdisciplinary Research on Climate version 5 (MIROC5) are the two models that exhibit realistic ENSO nonlinearity. With quadrupled atmospheric carbon dioxide, the ENSO amplitude of GFDL-ESM2M decreases by about 40%, whereas that of MIROC5 remains almost constant. Because GFDL-ESM2M exhibits stronger climatological thermal stratification than MIROC5, greenhouse gas forcing increases the upper ocean stability and causes the thermocline to be less sensitive to wind perturbations. The stiffer thermocline inhibits the nonlinear variations of sea surface temperature so that the ENSO amplitude substantially weakens. Idealized nonlinear recharge oscillator model experiments further support climatological thermal stratification as a determinant of the warming response. Observations exhibit stronger thermal stratification than both models, which suggests that the real world may terminate strong, nonlinear El Niños sooner than model-based projections.

Plain Language Summary The El Niño–Southern Oscillation (ENSO) is the most prominent mode of interannual natural variability that influences global-mean temperature, severe weather, tropical cyclone activity, marine ecosystems, and food production worldwide. Potential future changes in ENSO under global warming have been disputed, however, due to difficulty in reproducing the observed ENSO features by global climate models. *ENSO nonlinearity* (i.e., El Niño events tend to be stronger than La Niña events in the real world) is one of those difficult features. Here we show that ENSO nonlinearity, though not reproduced well by most state-of-the-art climate models, could play a major role in determining the ENSO response. We examine two climate models that successfully reproduce realistic ENSO nonlinearity to discuss potentially important physical processes. Our results support a notion that strong El Niño events may be terminated in the near future.

1. Introduction

The tropical Pacific Ocean has attracted attention in physical climatology, because its variability influences the climate all over the Earth (e.g., Horel & Wallace, 1981; Rasmusson & Wallace, 1983). The El Niño–Southern Oscillation (ENSO) is the dominant mode of interannual climate variability, so the response of ENSO to global warming is of great interest for the future climate (e.g., Christensen et al., 2013; Collins et al., 2010; Kim et al., 2014). State-of-the-art global climate models (GCMs), however, have difficulty reproducing the features of the observed ENSO, including its amplitude, irregular frequency, non-Gaussianity, and their impacts on the extratropics (e.g., Bellenger et al., 2014; Collins et al., 2010; Zhang & Sun, 2014). Weaknesses in the simulation of ENSO render large uncertainty in the warming response of the entire climate system (e.g., Christensen et al., 2013; Kohyama & Hartmann, 2016; Murakami et al., 2012; Yokoi & Takayabu, 2009).

Despite the difficulty of simulating ENSO, it has been common to choose a subset of GCMs that reproduce a particular observed feature well, and to assume that this subset makes more reliable future projections than the multimodel mean (e.g., Risbey et al., 2014). Based on this assumption, we project the future ENSO amplitude responses using two GCMs that realistically reproduce the observed ENSO nonlinearity, because of which warm anomalies tend to be larger than cold anomalies (El Niños tend to be stronger than La Niñas). Figure 1a shows the relationship between the ENSO skewness (a measure of the ENSO nonlinearity) and the zonal sea surface temperature (SST) gradient change simulated by GCMs under global warming. This figure shows that the Geophysical Fluid Dynamics Laboratory Earth System Model Version 2M (GFDL-ESM2M; Dunne et al., 2012; Dunne et al., 2013) and the Model for Interdisciplinary Research on Climate version 5 (MIROC5;

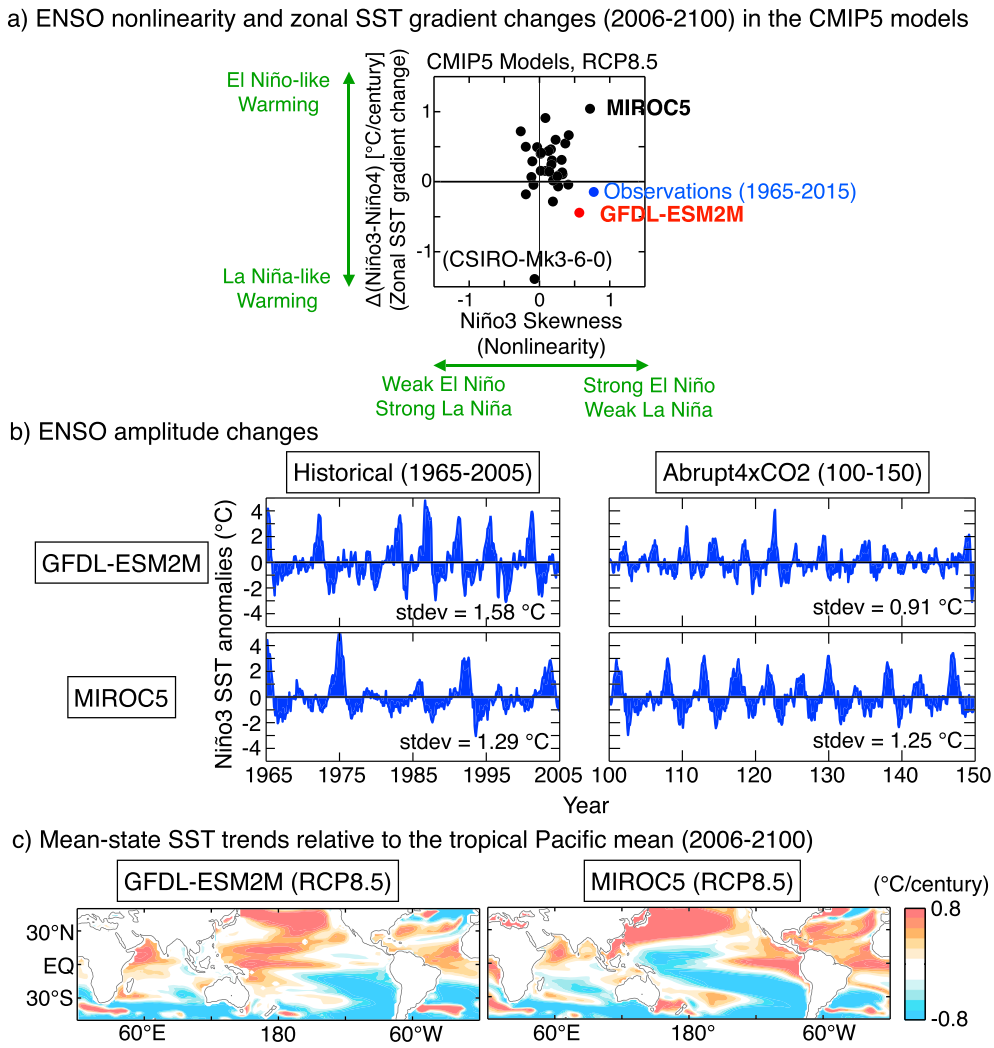

Figure 1. (a) Scatter plot showing the relationship between the Niño3 SST skewness and the zonal SST gradient change, the latter of which is defined as the linear trend of the regional mean SST difference calculated in the manner of *Niño3 minus Niño4*. Each dot represents the model output from (red) GFDL-ESM2M and (black) other CMIP5 models under the RCP8.5 scenario from 2006 to 2100, and (blue) observations from 1965 to 2015. Reproduced from Kohyama and Hartmann (2017). Copyright belongs to the American Meteorological Society. (b) Monthly Niño3 SST anomalies calculated for (top) GFDL-ESM2M and (bottom) MIROC5 under the (left) historical and (right) quadrupled CO_2 forcings. Standard deviations are shown at the bottom right. (c) SST warming trends under the RCP8.5 scenario from 2006 to 2100 of (left) GFDL-ESM2M and (right) MIROC5 calculated at each grid. Difference from the tropical Pacific mean trend (30°S to 30°N, 90°E to 60°W) is plotted. Red colors denote a warming faster than the tropical Pacific mean, and blue colors slower (i.e., not necessarily a cooling). ENSO = El Niño–Southern Oscillation; SST = sea surface temperature; CMIP5 = Coupled Model Intercomparison Project Phase 5; MIROC5 = Model for Interdisciplinary Research on Climate version 5; GFDL-ESM2M = Geophysical Fluid Dynamics Laboratory Earth System Model Version 2M; RCP = Representative Concentration Pathway.

Watanabe et al., 2010) are the two models that reproduce the observed ENSO skewness better than most of the other models that participated in the Coupled Model Intercomparison Project Phase 5 (CMIP5; Taylor et al., 2012). We analyze these two GCMs.

Figure 1b shows the time series of SST anomalies averaged over the Niño3 region (5°S to 5°N, 150°W to 90°W), a common index of ENSO. The left column shows the Niño3 SST for the historical climate of the two GCMs. Though GFDL-ESM2M exhibits an excessively large ENSO variance, both models exhibit realistic ENSO nonlinearity as suggested by Figure 1a. The right column shows the same time series but for a warmer climate. Interestingly, compared to the historical climate, the standard deviation of the Niño3 index of GFDL-ESM2M is reduced by about 40%, whereas that of MIROC5 remains almost constant in a warmer climate. Our motivations

are to understand this difference in the amplitude responses and to make a physically reasonable projection of the future ENSO change.

Recent studies that link the projected warming response in the mean-state tropical Pacific SST to the ENSO nonlinearity further motivate us to proceed in this vein. We hereafter call a mean-state response *El Niño-like* when the eastern equatorial Pacific warms faster than the west, and the opposite response *La Niña-like* (An et al., 2012; Collins, 2005; Held et al., 2010). The majority of the CMIP5 models project an El Niño-like warming response (e.g., Ying et al., 2016; Zheng et al., 2016), presumably because of the mechanism proposed by Held and Soden (2006) and Vecchi and Soden (2007). They argued that the hydrologic and energetic constraints robustly require the global-mean circulation to be weakened by global warming and that the weakened Walker circulation is expected to yield an El Niño-like response via reduced upwelling. As noted by Kohyama et al. (2017) and Kohyama and Hartmann (2017), however, a strengthened Walker circulation does not violate the requirement of the weakening *global-mean* circulation and hence their argument does not rule out a La Niña-like mean-state change.

There are several plausible mechanisms that could lead to a La Niña-like mean-state response to global warming (see Kohyama et al., 2017, for an extended discussion). If the mean climate is altered by a certain mechanism, it can potentially modulate the ENSO amplitude. For example, if the polar amplification is relatively weak, the equatorial upwelling water may remain cold, which favors a La Niña-like response and could weaken the ENSO amplitude. On the other hand, given realistic ENSO nonlinearity, changes in the amplitude of ENSO amplitude would also render a La Niña-like mean-state change. According to Kohyama et al. (2017), the important characteristic of GFDL-ESM2M appears to be that the ENSO nonlinearity is reduced under global warming, which rectifies the mean-state SST to be La Niña like. Because El Niños exhibit large amplitudes for the historical climate, whereas very few La Niñas go extreme, the El Niño amplitudes will be weakened more than that of La Niñas, if the ENSO nonlinearity is lost. This asymmetric weakening response would rectify the mean-state SST to become La Niña like, and this mechanism is referred to as the nonlinear ENSO warming suppression (NEWS). Kohyama and Hartmann (2017) concluded that a necessary condition to simulate NEWS is realistic ENSO skewness, and the lack thereof is why most CMIP5 models exhibit El Niño-like responses.

Realistic ENSO skewness, however, is not a sufficient condition to simulate NEWS. Figures 1a and 1c show that, though both GFDL-ESM2M and MIROC5 exhibit realistic ENSO skewness, MIROC5 exhibits a strong El Niño-like mean-state response unlike GFDL-ESM2M. This difference motivates us to understand why the ENSO nonlinearity is not the only requirement for a La Niña-like response.

This article is organized as follows. Data and methods are described in the next section. In section 3, we show that the response of SST to the thermocline depth anomalies is the source of the ENSO nonlinearity in these models. Then, we propose a nonlinear mechanism for how the climatological upper ocean thermal stratification determines the ENSO amplitude response to warming. We also compare the observed thermal stratification with the modeled ones. Conclusions are presented in section 4.

2. Data and Methods

2.1. Data

The monthly surface temperature, oceanic potential temperature, and wind stress output of GFDL-ESM2M (Dunne et al., 2012; Dunne et al., 2013) are from the GFDL Data Portal (http://nomads.gfdl.noaa.gov:8080/DataPortal/cmip5.jsp), and those of MIROC5 (Watanabe et al., 2010) are from the Program for Climate Model Diagnosis and Intercomparison (https://pcmdi.llnl.gov/projects/cmip5/). We analyze the first ensemble member of the historical (Years 1966–2005) and abrupt4xCO_2 runs (Years 101–150 after the abrupt change are used). In the Abrupt4xCO_2 runs, Year 101 starts when 100 years have passed after the abrupt quadrupling of carbon dioxide, and the qualitative argument regarding the ENSO amplitude is not sensitive to this choice of the 50-year time span (see also Kohyama & Hartmann, 2017). We are aware that even without anthropogenic forcing, the variance of ENSO over a 50-year span will differ simply due to natural variability (Wittenberg, 2009). Kohyama et al. (2017) and Kohyama and Hartmann (2017), however, showed that the ENSO amplitude in GFDL-ESM2M is kept suppressed for at least 200 years under the 4xCO2 forcing, in addition to confirming that the Representative Concentration Pathway (RCP) 6.5 (95 years), RCP 8.5 (95 years), and 1percentCO2 (200 years) runs also exhibit well-defined La Niña-like trends. Therefore, though we have to regard the limited sample size as a caveat, we have sufficient evidence to support a notion that the ENSO change discussed in this study is forced and not a sampling problem. At each depth, the oceanic variables are regridded using linear

interpolation onto a 2.5° longitude by 2° latitude grid. To produce Figure 1, the first ensemble member of the RCP 8.5 (Years 2006–2100) runs are used. Detailed descriptions of the CMIP5 project are presented by Taylor et al. (2012).

The reanalysis monthly oceanic potential temperature is from the National Centers for Environmental Prediction Global Ocean Data Assimilation System (Behringer & Xue, 2004) at http://www.esrl.noaa.gov/psd/data/gridded/data.godas.html. The horizontal resolution is 1° longitude by 1/3° latitude, and the vertical resolution is 10 m for uppermost 230 m and becomes coarser toward the deeper levels. The SST and zonal wind stress are from the European Centre for Medium range Weather Forecasting ERA-Interim reanalysis data (Dee et al., 2011). The SST is downloaded from http://apps.ecmwf.int/datasets/data/interim-full-moda/levtype=sfc/, and the zonal wind stress is from https://climexp.knmi.nl/start.cgi. The time span used in this study is from 1980 to 2016 for all the reanalysis data.

2.2. Methods

2.2.1. Decomposing the Sources of the ENSO Nonlinearity

Following An and Kim (2017) and Lübbecke and McPhaden (2017), we decompose the source of the ENSO nonlinearity into three components: (i) *SST modulates winds*, (ii) *winds excite oceanic waves*, and (iii) *oceanic waves that have propagated to the east modulate SST*. To close the Bjerknes feedback loop, we look at SST in (iii), following Lübbecke and McPhaden (2017), rather than subsurface temperature as An and Kim (2017) did, though our conclusions do not depend on this choice. To measure the relative impact of these three sources of nonlinearity, we draw scatter plots between two area-averaged anomalies in the manner of (i) SST (170–120°W, 5°S to 5°N) and zonal wind stress (120°E to 80°W, 5°S to 5°N); (ii) zonal wind stress (120°E to 80°W, 5°S to 5°N) and thermocline depth (120°E to 80°W, 5°S to 5°N); (iii) eastern thermocline depth (170–120°W, 5°S to 5°N) and SST (170–120°W, 5°S to 5°N). These anomalies are deviations from monthly climatology calculated as the average over the full time span for each calendar month. The thermocline depth is defined as the level of maximum vertical temperature gradient. To draw each scatter plot, we first calculate the lead-lag relationship between the two variables and choose the lags with maximum correlations.

The best fit lines are drawn based on the standardized data. Linear regression and principle component analysis yield almost identical linear fits. In Figure 2, following An and Kim (2017), the asymmetry index is defined as

$$Asym = \frac{S_p - S_n}{S_p + S_n} \tag{1}$$

where S_p (S_n) is the slope of the red (blue) best fit lines calculated using data with the positive-only (negative-only) values in the horizontal axis. Figure 2 displays the relationships after normalizing variables by their standard deviations, while Figures 3b and 3e show the relationships in physical units.

2.2.2. Idealized Model

We use a modified version of the heuristic nonlinear recharge oscillator ENSO model introduced by Jin (1998) and Timmermann et al. (2003). This model is a simplified, two-box approximation of the Cane-Zebiak model (Zebiak & Cane, 1987). Detailed descriptions of the model and our modifications are given in Kohyama and Hartmann (2017).

3. Results

3.1. Source of the ENSO Nonlinearity

Figure 2a shows the observed three potential sources of ENSO nonlinearity. Among the three, the asymmetry index is largest for (iii), so the observational ENSO nonlinearity mainly originates from the SST response to oceanic waves. This result is consistent with Lübbecke and McPhaden (2017) but may appear inconsistent with An and Kim (2017) who showed that (ii) is the major source of the nonlinearity. This inconsistency may originate from data set dependence and/or detailed analysis procedures, which we have to leave as a caveat, but not from using SST in place of subsurface temperature. We have confirmed that using subsurface temperature yields almost identical results.

Figure 2b shows the same scatter plots but for the historical runs of GFDL-ESM2M and MIROC5. These two GCMs reproduce the observed relationships of (i)–(iii) well, suggesting that the source of the nonlinearity in these models are (iii). The responses to increasing CO_2 are different between the two GCMs, however. Figure 2c shows the same plots but for the warmer climate, where the (iii) component becomes virtually linear

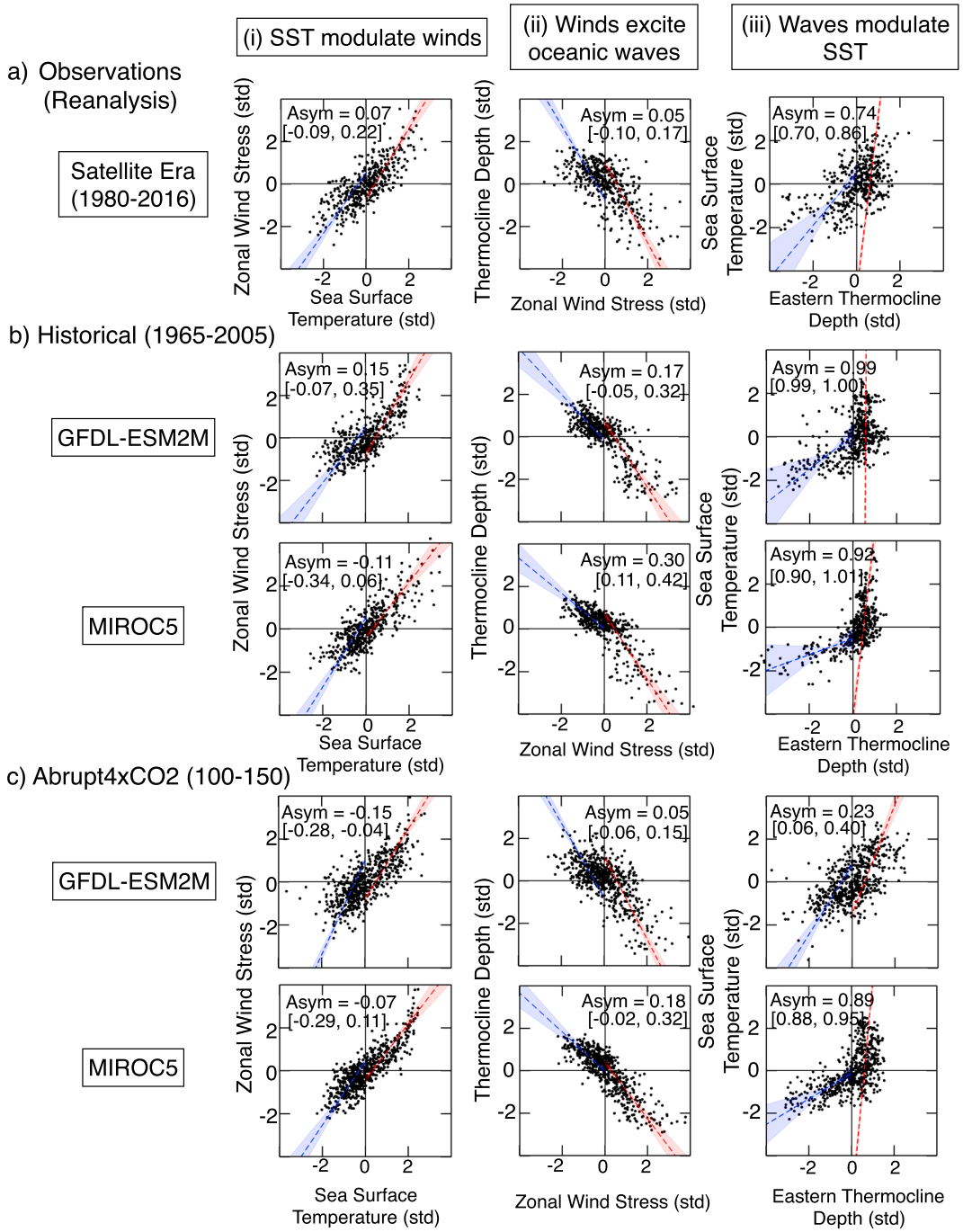

Figure 2. (a) Scatter plots of observed, lagged anomalies between monthly area-averaged standardized time series of (left) SST and zonal wind stress, (middle) zonal wind stress and thermocline depth, and (right) eastern thermocline depth and SST. Lags are chosen to realize the maximum correlations. The red (blue) best fit lines are calculated using the data only with the positive (negative) values in the horizontal axis. The shaded areas show the estimated ranges of the true regression slopes at the 95% confidence level. The asymmetry index defined in equation (1) is shown at the top of each panel. The numbers in the brackets are the (left) lower and (right) upper bounds of the asymmetry indices calculated from the estimated ranges of the slopes. (b) As in (a) but for (top) GFDL-ESM2M and (bottom) MIROC5 under the historical forcing. (c) As in (b) but for the quadrupled CO_2 forcing. SST = sea surface temperature; GFDL-ESM2M = Geophysical Fluid Dynamics Laboratory Earth System Model Version 2M; MIROC5 = Model for Interdisciplinary Research on Climate version 5.

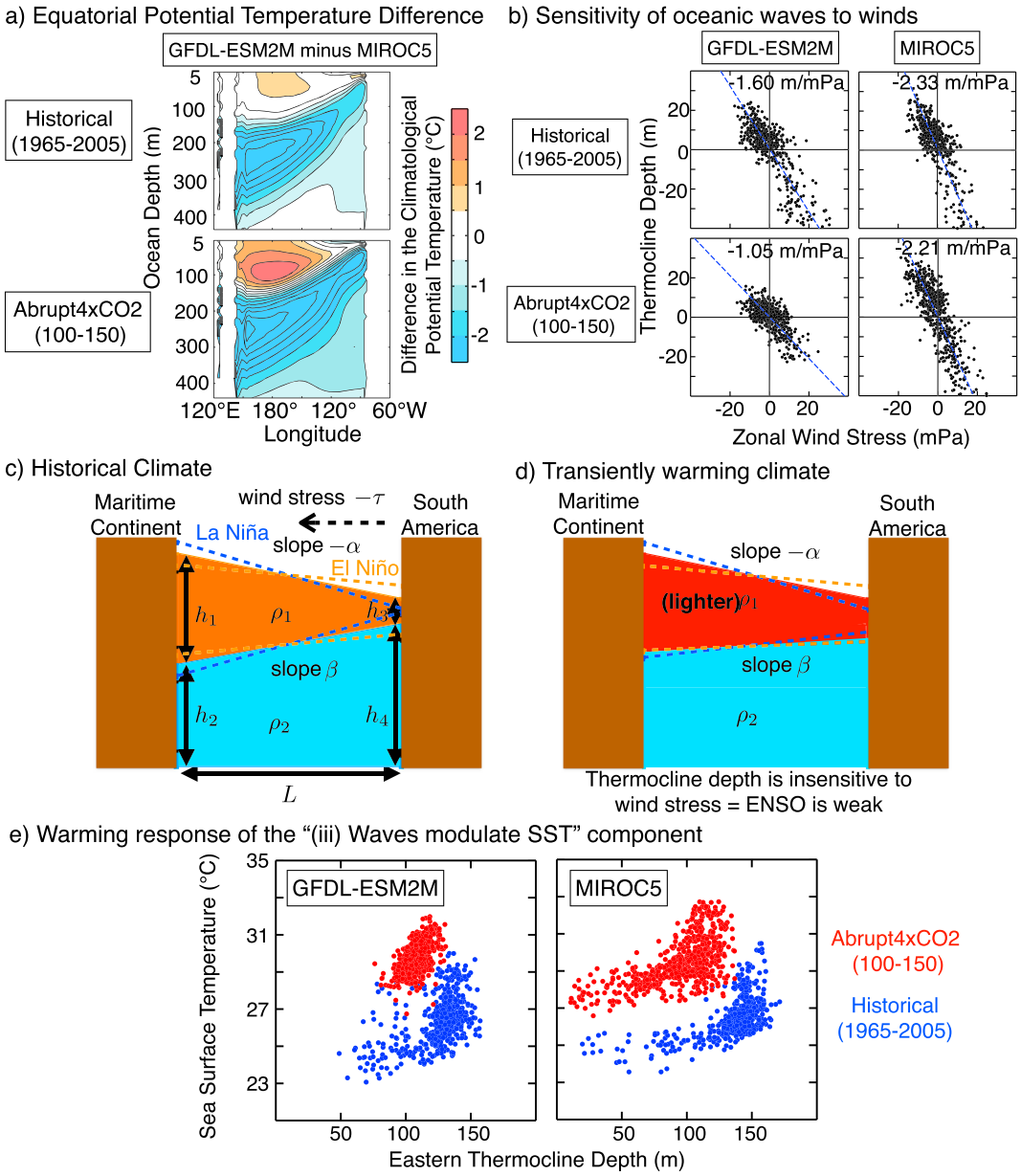

Figure 3. (a) Difference in climatological oceanic potential temperature averaged over 5°S to 5°N in the manner of GFDL-ESM2M minus MIROC5 under the (top) historical and (bottom) quadrupled CO_2 forcings. (b) As in the middle column of (top) Figures 2b and (bottom) 2c, but with physical units. The blue dashed best fit lines are calculated using the entire data (rather than only positive or negative anomalies as in Figure 2), and the slopes are shown at the top. (c) Schematic showing the relationship between the slope of the ocean surface and thermocline for the historical climate. Each variable is defined in section 3.2 (d) As in (c) but for a transiently warming climate. Red color denotes warmer and lighter sea water than (c), which makes the thermocline depth insensitive to wind stress input, inducing weaker El Niño–Southern Oscillation. (e) As in the right column of Figures 2b and 2c but with physical units. Output from the (blue) historical and (red) quadrupled CO_2 experiments of (left) GFDL-ESM2M and (right) MIROC5 are plotted. GFDL-ESM2M = Geophysical Fluid Dynamics Laboratory Earth System Model Version 2M; MIROC5 = Model for Interdisciplinary Research on Climate version 5; SST = sea surface temperature.

in GFDL-ESM2M but not in MIROC5. The asymmetry index of (iii) in GFDL-ESM2M changes from 0.99 to 0.23 with warming, whereas in MIROC5 only from 0.92 to 0.89. Though the mechanism for the ENSO nonlinearity for the historical climate is similar between the two models, the warming response of nonlinearity is different.

3.2. Mechanism for the Different ENSO Warming Responses

Kohyama and Hartmann (2017) concluded that the climatological temperature difference between the atmosphere near the surface and the ocean below the thermocline serves as a determinant of the nonlinear response to warming. Therefore, we first compare the climatological upper ocean temperature between the two models.

Figure 3a shows the equatorial climatological temperature difference between the two models. For the historical climate, temperature below the thermocline is cooler in GFDL-ESM2M than in MIROC5, whereas temperature above the thermocline is warmer (Figure 3a, top). That is, the equatorial ocean interior is more thermally stratified and stable in GFDL-ESM2M than in MIROC5. This difference in the stability becomes more evident in the warmer experiment (Figure 3a, bottom). This intensification of the stability difference under global warming may be due to a positive feedback as follows. If the ocean is more stable, the warmer water in the upper ocean is less likely to be vertically mixed with the colder water in the deeper ocean. The suppressed vertical heat exchange further stabilizes the system.

If the ocean becomes more stable, the equatorial thermocline becomes less sensitive to winds due to the following mechanism. Figure 3c shows a schematic of the equatorial thermocline presented as a 1.5-layer model. Hydrostatic balance and no motion in the lower layer are assumed, because in principle, no energy enters the lower layer at sufficiently high frequencies. Hence, the pressure gradient at a reference level in the lower layer is zero:

$$\rho_1 h_1 + \rho_2 h_2 = \rho_1 h_3 + \rho_2 h_4 \tag{2}$$

or

$$\rho_1 \frac{h_1 - h_3}{L} = \rho_2 \frac{h_4 - h_2}{L} \tag{3}$$

where L denotes the width of the basin in the longitudinal direction, ρ_1 (ρ_2) denotes the upper (lower) layer density, and h_i denotes the layer depth. For h_i, the index i denotes the upper (lower) layer by $i = 1, 3$ ($i = 2, 4$), and the western (eastern) edge of the basin by $i = 1, 2$ ($i = 3, 4$) as described in Figure 3c. Using the definition of the slopes, $-\alpha \equiv \{(h_3 + h_4) - (h_1 + h_2)\}/L$ and $\beta \equiv (h_4 - h_2)/L$ where $\alpha > 0$, $\beta > 0$, we get

$$\rho_1(\alpha + \beta) = \rho_2 \beta \tag{4}$$

or

$$\beta = \frac{\alpha}{\rho_2/\rho_1 - 1} \tag{5}$$

Differentiating both sides, and assuming that the easterly wind stress anomalies ($-d\tau$) is proportional to the sea level tilt anomalies ($d\alpha \propto -d\tau$; Li & Clarke, 1994), we get

$$\mathrm{d}\beta \propto -\frac{\mathrm{d}\tau}{\rho_2/\rho_1 - 1} \tag{6}$$

Equation (6) means that the sensitivity of the thermocline tilt anomalies to wind stress, or $1/(\rho_2/\rho_1 - 1)$, depends upon the ratio of the densities between the two layers. Therefore, if the ocean becomes more stable as the climate warms, the denominator $\rho_2/\rho_1 - 1$ becomes larger and the equatorial thermocline depth becomes less sensitive to winds, as schematically shown in Figure 3d. Using the reduced gravity $g' = g(\rho_2/\rho_1 - 1)$, equation (6) could be also written as

$$\mathrm{d}\beta \propto -\frac{\mathrm{d}\tau}{g'} \tag{7}$$

where the constant g is omitted. Equations (6) and (7) both indicate that the thermocline slope is less sensitive to wind stress for a more stable ocean.

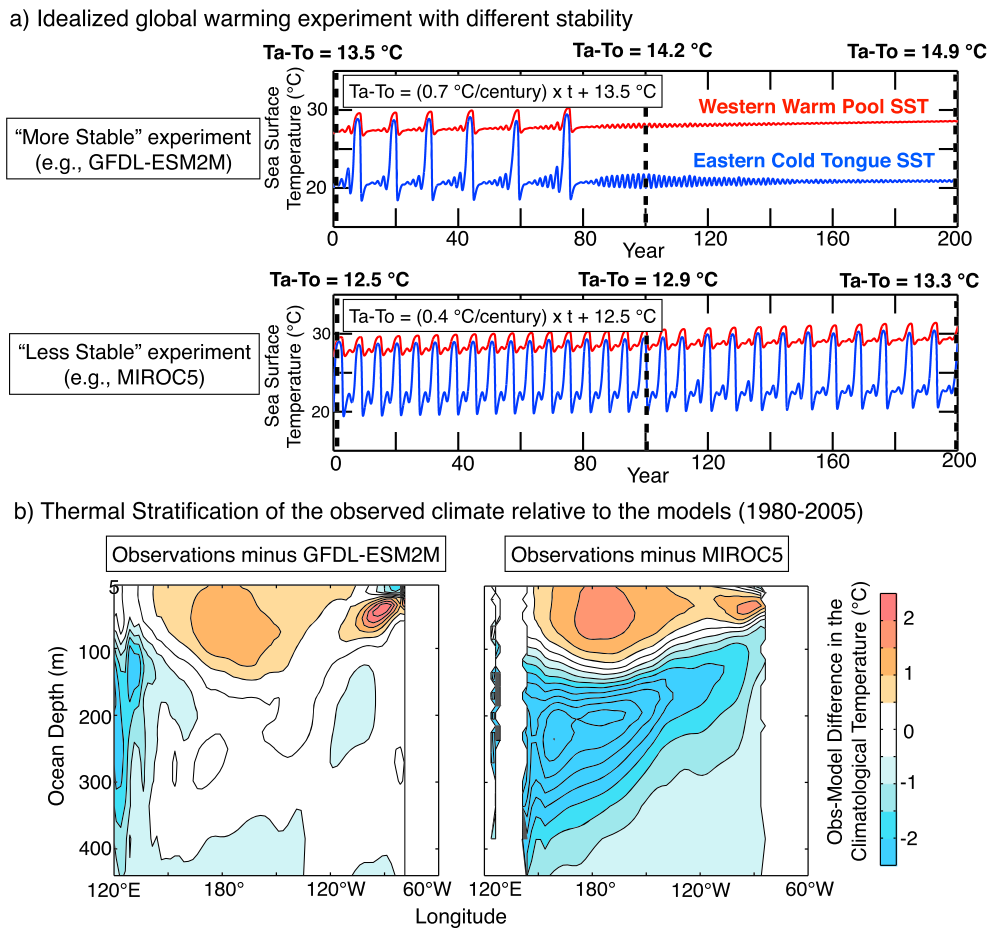

Figure 4. (a) Idealized model experiments that simulate the (red) western and (blue) eastern equatorial Pacific SST variability. The climatological reservoir temperature difference between the atmosphere near the surface and the ocean below the thermocline ($T_a - T_o$) is linearly increased with the rate of (top) 0.7 °C per century starting at $T_a - T_o$=13.5 °C and (bottom) 0.4 °C per century starting at $T_a - T_o$=12.5 °C, which represent two types of models with stronger and weaker upper ocean thermal stratifications, respectively. $T_a - T_o$ in Years 0, 100, and 200 are shown at the top of each panel. (b) Left: As in Figure 3a but the difference calculated in the manner of reanalysis minus GFDL-ESM2M in the late historical period (1980-2005). Right: As in left but reanalysis minus MIROC5. GFDL-ESM2M = Geophysical Fluid Dynamics Laboratory Earth System Model Version 2M; MIROC5 = Model for Interdisciplinary Research on Climate version 5; SST = sea surface temperature.

Based on this mechanism, the sensitivity of thermocline to winds shown in Figure 3b is consistent with the thermal stratification shown in Figure 3a. For the historical climate, GFDL-ESM2M has a more stable ocean and exhibits a smaller sensitivity of the thermocline to winds than MIROC5 by about 30%. We could call the thermocline in GFDL-ESM2M *stiffer* than in MIROC5. For the warmer climate, the difference in thermocline sensitivity between the two models becomes larger, because the upper ocean in GFDL-ESM2M warms faster and the stability is increased more.

Because the thermocline in GFDL-ESM2M is stiffer in the warmer climate, equatorial waves with large amplitudes are harder to excite, and the resultant modulations of the eastern thermocline are reduced. Figure 3e robustly shows that, in the warmer experiment in GFDL-ESM2M, SST does not *swing* enough to support large ENSO events due to the weaker wave displacements. The weak wave displacements appear to be why the ENSO in GFDL-ESM2M becomes almost linear for the warmer climate. In MIROC5, however, the variations of the eastern thermocline are kept large enough to sustain the nonlinear response of SST. Due to the weak historical thermal stratification, the thermal stratification in MIROC5 does not become stronger as rapidly as in GFDL-ESM2M. Due to the small stability, the thermocline responds strongly to winds. This more *reactive* thermocline allows larger anomalies to enter the eastern thermocline, which supports strong, nonlinear SST variations.

In Figure S1 in the supporting information, we show the results from the Community Climate System Model version 4 (CCSM4; Gent et al., 2011), which exhibits similar thermal stratification as GFDL-ESM2M but with weaker nonlinearity. The increased stratification and reduced ENSO variance is also seen in CCSM4 but to a less extent than in GFDL-ESM2M because of the weaker mean-state nonlinearity in CCSM4. Compared to GFDL-ESM2M, the nonlinear rectification effect on the mean-state SST is also limited. We examined four additional CMIP5 models, but these models do not exhibit the physical processes that we discuss in this paper due to the lack of realistic nonlinearity. Therefore, we should remark as a caveat that we have focused mostly on the two models with best ENSO nonlinearity in this particular study, so the robustness of our conclusions concerning the future ENSO variability is limited due to the limited number of models with more realistic ENSO nonlinearity.

3.3. Idealized Model Experiments

To illustrate the mechanism by numerical simulations, we have performed two idealized model experiments with different stability. In the *More Stable* experiment (Figure 4a, top), the temperature difference between the atmosphere near the surface and the ocean below the thermocline ($T_a - T_o$) is initially set to be 13.5 °C, and the $T_a - T_o$ is increased with the rate of 0.7 °C per century, expressing that the atmosphere warms faster than the ocean due to the different heat capacity. In the *Less Stable* experiment (Figure 4a, bottom), $T_a - T_o$ is initially set to be 12.5 °C, and the $T_a - T_o$ is increased with the rate of 0.4 °C per century. The $T_a - T_o$ is increased more rapidly in the More Stable experiment to incorporate the effect of the suppressed vertical heat exchange.

Figure 4a shows the SST time series in the two experiments. In the More Stable experiment, which is designed to imitate GFDL-ESM2M, strong El Niños are terminated at the threshold of $T_a - T_o \sim 14.2$ °C. This termination is because the *stiff* thermocline cannot redistribute as much heat in the equatorial upper ocean to yield a strong El Niño (Kohyama & Hartmann, 2017). By contrast, in the Less Stable experiment, which is designed to imitate MIROC5, strong El Niños are not terminated because $T_a - T_o$ does not reach the threshold of ~ 14.2 °C even after the two-century run. Rather, because of the warming western Pacific, which serves as the upper bound of the ENSO intensity (An & Jin, 2004), the ENSO amplitude strengthens by about 10% during the two centuries. This difference in the existence of the nonlinearity termination between the two experiments is consistent with the mechanism explained in the previous subsection.

3.4. Comparison With Observations

We also compare the two models with the observations to project the future ENSO change. Figure 4b shows the same temperature plot as in Figure 3a but for observations relative to the two models. The observed equatorial upper ocean is more stable than the GFDL-ESM2M, which is more stable than MIROC5. This observed strong stability is more favorable for $T_a - T_o$ to reach the threshold that terminates strong El Niño events than in the two models. Though this conclusion is derived only from the two GCMs and idealized model experiments, it makes physical sense to project that, based on the observations and the available models with realistic nonlinearity, ENSO may weaken nonlinearly sooner than the model-based projections.

4. Conclusions

4.1. The ENSO Nonlinearity Matters to the ENSO and Mean-State Responses to Global Warming

Under global warming, the ENSO amplitude in GFDL-ESM2M weakens, but that in MIROC5 remains almost constant (Figure 1b). Decomposing the potential source of the ENSO nonlinearity into three components, we have demonstrated that the difference in the ENSO amplitude responses between the two models is associated with the nonlinear SST response to oceanic waves, rather than the wind response to SST or the oceanic wave response to winds (Figures 2 and 3e).

Many GCMs show strengthening of ENSO in response to warming (Collins et al., 2010), but they do not reproduce the ENSO nonlinearity as realistically as GFDL-ESM2M and MIROC5 (Figure 1a). Our preliminary analysis suggests that many CMIP5 models do not reproduce the nonlinear SST response to waves. Without the possibility of the nonlinear regime shift, one might project that the ENSO amplitude will strengthen. We should, however, pay more attention to the GCMs that reproduce the realistic ENSO nonlinearity, because ENSO in the real world is nonlinear.

Based on the NEWS mechanism (Kohyama & Hartmann, 2017), the nonlinear ENSO response to global warming can rectify the mean-state SST. Therefore, the difference of the nonlinear ENSO response between GFDL-ESM2M and MIROC5 could have an important implication for whether the response will be El Niño

like or La Niña like (Figure 1). Considering the scientific and societal impacts, the ENSO nonlinearity is a key characteristic and should not be considered to be a minor, higher-order correction of the linear ENSO.

4.2. An Urgent Task Is to Improve the Reproducibility of the Thermal Stratification in GCMs Because It Determines the Nonlinear ENSO Response

With strong climatological thermal stratification in the upper ocean, ENSO may weaken nonlinearly in response to warming. The mechanism is explained as follows. If the thermal stratification becomes stronger, weaker thermocline variations can keep the ocean in hydrostatic balance (Figures 3c and 3d and equation (6). The resultant stiffer thermocline depth is less sensitive to winds (Figure 3b), which minimizes the nonlinear response of the eastern SST. Importantly, despite the small difference in thermocline sensitivity, the nonlinearity produces a huge difference in the amplitude of SST (Figure 3e).

The idealized model confirms that the climatological temperature difference between the atmosphere near the surface and the ocean below the thermocline ($T_a - T_o$) is an important parameter (Figure 4a). Here $T_a - T_o$ could be regarded as the first-order approximation of the climatological thermal stratification. Once $T_a - T_o$ reaches a certain threshold value, strong El Niños become terminated (see also ; Kohyama & Hartmann, 2017). This sudden loss of strong El Niños is consistent with the two GCMs. In GFDL-ESM2M, because the thermal stratification is strong, ENSO becomes almost linear. By contrast, ENSO keeps its amplitude in MIROC5, because the weak thermal stratification is unfavorable to reach the threshold for the ENSO to weaken. It might be interesting to warm MIROC5 more and check whether the ENSO in MIROC5 can be weakened.

The differences in vertical stratification in these two models could be due to a myriad of differences in the models, including the background diffusivity, the shear mixing scheme, the boundary layer scheme, the vertical resolution, and the mixing due to truncation errors. Hence, it is not possible to discern the cause(s) for the difference in the vertical stratification between GFDL-ESM2M and MIROC5. More analysis and numerical simulations are needed to understand the model difference.

4.3. Observational Thermal Stratification Suggests That the ENSO Amplitude Might Weaken Nonlinearly, and the Regime Shift Might Happen Sooner Than the GCM-Based Projections

GFDL-ESM2M and MIROC5 suggests that, if $T_a - T_o$ is large for the historical climate, $T_a - T_o$ will increase rapidly under a warming climate (Figure 3a). This intensification of $T_a - T_o$ makes physical sense, because the suppressed vertical mixing will inhibit the vertical heat exchange. As shown in Figure 4b, the observed $T_a - T_o$ is larger than the modeled ones for the historical climate. Therefore, the observed strong $T_a - T_o$ may support a rapid increase of $T_a - T_o$ that terminates strong El Niños. GFDL-ESM2M exhibits the termination of strong El Niños in Year 2070 for the RCP8.5 scenario (Kohyama & Hartmann, 2017), so the observed strong thermal stratification leads us to speculate that the regime shift might happen in a couple of decades.

Acknowledgments
This study is based on data from the GFDL Data Portal (http://nomads.gfdl.noaa.gov:8080/DataPortal/cmip5.jsp), the Program for Climate Model Diagnosis and Intercomparison website (https://pcmdi.llnl.gov/projects/cmip5/), and the GODAS data set (http://www.esrl.noaa.gov/psd/data/gridded/data.godas.html). This work was supported by the National Science Foundation (NSF) under grant AGS-1549579 and Takenaka Scholarship Foundation. The third author was funded by the Tamaki Foundation. We would like to thank Michiya Hayashi and Tomoki Tozuka for their useful advice.

References

An, S.-I., & Jin, F.-F. (2004). Nonlinearity and asymmetry of ENSO. *Journal Climate*, *17*, 2399–2412.

An, S.-I., & Kim, J.-W. (2017). Role of nonlinear ocean dynamic response to wind on the asymmetrical transition of El Niño and La Niña. *Geophysical Research Letters*, *44*, 393–400. https://doi.org/10.1002/2016GL071971

An, S.-I., Kim, J. W., Im, S.-H., Kim, B.-M., & Park, J.-H. (2012). Recent and future sea surface temperature trends in tropical Pacific warm pool and cold tongue regions. *Climate Dynamics*, *39*(6), 1373–1383.

Behringer, D. W., & Xue, Y. (2004). Evaluation of the global ocean data assimilation system at NCEP: The Pacific Ocean. In *Proc. eighth symp. on integrated observing and assimilation systems for atmosphere, oceans, and land surface*.

Bellenger, H., Guilyardi, É., Leloup, J., Lengaigne, M., & Vialard, J. (2014). ENSO representation in climate models: From CMIP3 to CMIP5. *Climate Dynamics*, *42*(7-8), 1999–2018.

Christensen, J. H., Krishna Kumar, K., Aldrian, E., An, S.-I., Cavalcanti, I. F. A., deCastro, M., et al. (2013). Climate phenomena and their relevance for future regional climate change. In T. F. Stocker, et al. (Eds.), *Climate Change 2013: The Physical Science basis. Contribution of Working Group I to the Fifth Assessment Report of the Intergovernmental Panel on Climate Change* (pp. 1217–1308). Cambridge, UK and New York: Cambridge University Press.

Collins, M. (2005). El Niño-or La Niña-like climate change? *Climate Dynamics*, *24*(1), 89–104.

Collins, M., An, S.-I., Cai, W., Ganachaud, A., Guilyardi, E., Jin, F.-F., et al. (2010). The impact of global warming on the tropical Pacific Ocean and El Niño. *Nature Geoscience*, *3*(6), 391–397.

Dee, D. P., Uppala, S. M., Simmons, A. J., Berrisford, P., Poli, P., Kobayashi, S., et al. (2011). The ERA-Interim reanalysis: Configuration and performance of the data assimilation system. *Quarterly Journal of the Royal Meteorological Society*, *137*, 553–597. https://doi.org/10.1002/qj.828

Dunne, J. P., John, J. G., Adcroft, A. J., Griffies, S. M., Hallberg, R. W., Shevliakova, E., et al. (2012). GFDL's ESM2 global coupled climate-carbon Earth System Models. Part I: Physical formulation and baseline simulation characteristics. *Journal Climate*, *25*(19), 6646–6665.

Dunne, J. P., John, J. G., Shevliakova, E., Stouffer, R. J., Krasting, J. P., Malyshev, S. L., et al. (2013). GFDL's ESM2 global coupled climate–Carbon Earth System Models. Part II: Carbon system formulation and baseline simulation characteristics. *Journal Climate*, *26*(7), 2247–2267.

Gent, P. R., Danabasoglu, G., Donner, L. J., Holland, M. M., Hunke, E. C., Jayne, S. R., et al. (2011). The Community Climate System Model version 4. *Journal of Climate*, *24*(19), 4973–4991.

Held, I. M., & Soden, B. J. (2006). Robust responses of the hydrological cycle to global warming. *Journal Climate*, *19*(21), 5686–5699.
Held, I. M., Winton, M., Takahashi, K., Delworth, T., Zeng, F., & Vallis, G. K. (2010). Probing the fast and slow components of global warming by returning abruptly to preindustrial forcing. *Journal Climate*, *23*(9), 2418–2427.
Horel, J. D., & Wallace, J. M. (1981). Planetary-scale atmospheric phenomena associated with the Southern Oscillation. *Monthly Weather Review*, *109*(4), 813–829.
Jin, F.-F. (1998). A simple model for the Pacific cold tongue and ENSO. *Journal of the Atmospheric Sciences*, *55*(14), 2458–2469.
Kim, S. T., Cai, W., Jin, F.-F., Santoso, A., Wu, L., Guilyardi, E., & An, S.-I. (2014). Response of El Niño sea surface temperature variability to greenhouse warming. *Nature Climate Change*, *4*(9), 786–790.
Kohyama, T., & Hartmann, D. L. (2016). Antarctic sea ice response to weather and climate modes of variability. *Journal Climate*, *29*(2), 721–741.
Kohyama, T., & Hartmann, D. L. (2017). Nonlinear ENSO Warming Suppression (NEWS). *Journal Climate*, *30*(11), 4227–4251.
Kohyama, T., Hartmann, D. L., & Battisti, D. S. (2017). La niña–like mean-state response to global warming and potential oceanic roles. *Journal Climate*, *30*(11), 4207–4225.
Li, B., & Clarke, A. J. (1994). An examination of some ENSO mechanisms using interannual sea level at the eastern and western equatorial boundaries and the zonally averaged equatorial wind. *Journal of Physical Oceanography*, *24*(3), 681–690.
Lübbecke, J. F., & McPhaden, M. J. (2017). Symmetry of the Atlantic Niño mode. *Geophysical Research Letters*, *44*, 965–973. https://doi.org/10.1002/2016GL071829
Murakami, H., Mizuta, R., & Shindo, E. (2012). Future changes in tropical cyclone activity projected by multi-physics and multi-sst ensemble experiments using the 60-km-mesh MRI-AGCM. *Climate Dynamics*, *39*(9-10), 2569–2584.
Rasmusson, E. M., & Wallace, J. M. (1983). Meteorological aspects of the El Niño/Southern Oscillation. *Science*, *222*(4629), 1195–1202.
Risbey, J. S., Lewandowsky, S., Langlais, C., Monselesan, D. P., OKane, T. J., & Oreskes, N. (2014). Well-estimated global surface warming in climate projections selected for ENSO phase. *Nature Climate Change*, *4*(9), 835–840.
Taylor, K. E., Stouffer, R. J., & Meehl, G. A. (2012). An overview of CMIP5 and the experiment design. *Bulletin of the American Meteorological Society*, *93*(4), 485–498.
Timmermann, A., Jin, F.-F., & Abshagen, J. (2003). A nonlinear theory for El Niño bursting. *Journal of the Atmospheric Sciences*, *60*(1), 152–165.
Vecchi, G. A., & Soden, B. J. (2007). Global warming and the weakening of the tropical circulation. *Journal Climate*, *20*(17), 4316–4340.
Watanabe, M., Suzuki, T., Oishi, R., Komuro, Y., Watanabe, S., Emori, S., et al. (2010). Improved climate simulation by MIROC5: Mean states, variability, and climate sensitivity. *Journal Climate*, *23*(23), 6312–6335.
Wittenberg, A. T. (2009). Are historical records sufficient to constrain ENSO simulations? *Geophysical Research Letters*, *36*(12), L12702. https://doi.org/10.1029/2009GL038710
Ying, J., Huang, P., & Huang, R. (2016). Evaluating the formation mechanisms of the equatorial Pacific SST warming pattern in CMIP5 models. *Advances in Atmospheric Sciences*, *33*(4), 433–441.
Yokoi, S., & Takayabu, Y. N. (2009). Multi-model projection of global warming impact on tropical cyclone genesis frequency over the western North Pacific. *Journal of the Meteorological Society of Japan*, *87*(3), 525–538.
Zebiak, S. E., & Cane, M. A. (1987). A model El Niño-Southern Oscillation. *Monthly Weather Review*, *115*(10), 2262–2278.
Zhang, T., & Sun, D.-Z. (2014). ENSO asymmetry in CMIP5 models. *Journal Climate*, *27*(11), 4070–4093.
Zheng, X.-T., Xie, S.-P., Lv, L.-H., & Zhou, Z.-Q. (2016). Inter-model uncertainty in ENSO amplitude change tied to Pacific ocean warming pattern. *Journal Climate*, *29*, 7265–7279.